IOP Publishing Journal of Physics B: Atomic, Molecular and Optical Physics
J. Phys. B: At. Mol. Opt. Phys. **47** (2014) 215003 (10pp) doi:10.1088/0953-4075/47/21/215003

Comparison of different quantum mechanical methods for inner atomic shell photo-ionization followed by Auger decay

Qianxia Wang[1], S Sheinerman[2] and F Robicheaux[3]

[1] Department of Physics, Auburn University, AL 36849, USA
[2] Department of Physics, St. Petersburg State Maritime Technical University, 198262 St. Petersburg, Russia
[3] Department of Physics, Purdue University, IN 47907, USA

E-mail: robichf@purdue.edu

Received 20 April 2014, revised 7 September 2014
Accepted for publication 12 September 2014
Published 15 October 2014

Abstract

A numerical time-dependent quantum mechanical approach was developed previously for simulating the process of photoionization followed by Auger decay for cases where the photoelectron energy is not very large; the method accurately calculates the interaction between the two active electrons, but simplifies their interaction with the core electrons. More established theoretical methods, which take account of postcollision interaction effects, allow an accurate description of this process when the photoelectron energy is not too low. We demonstrate that using the time-dependent method (although with some simplifications that are needed for its numerical implementation) for low energy photoelectrons and more established methods for higher energy allows accurate calculations for nearly all possible combinations of electron energy. This is confirmed by performing calculations of the photoelectron energy and angular distributions for the 1 s photoionization of Ne, with a subsequent KLL Auger transition. By computing the energy and angular distributions for energies where the two groups of methods should agree and where they should disagree, we demonstrate their consistency and range of accuracy. For the regions where the methods disagree, we discuss the reasons for any discrepancies and the trends in the differences. In addition, some of our calculations are compared with existing experimental data for the same system. The agreement found in the comparison confirms the reliability of the theoretical approaches.

Keywords: photo-ionization, auger decay, post-collision interaction

1. Introduction

The phenomenon of photoionization followed by Auger decay has been extensively studied in the past few decades, both theoretically [1–21] and experimentally [20, 22–34]. This is an interesting system to study for several reasons. Firstly, the Auger decay distorts the photoelectron energy distribution. The energy distribution becomes broader, and the maximum decreases and is shifted to smaller energy because of the abrupt increase in the ion's charge upon the Auger decay occurring. This phenomenon is one example of a postcollision interaction (PCI) effect [7]. PCI implies taking account of an interaction between the photoelectron, the Auger electron and the ion field which varies during the Auger decay. This system is also interesting because the strong interaction between the two ionized electrons distorts the distribution of the angle between the two ionized electrons. The two electrons interact with each other strongly, particularly when the electron emitted later in time has greater energy and, thus, must pass the electron emitted earlier. A third reason for interest is that the photoelectron which has been ionized may be recaptured to a bound state of the ion due to the PCI effect [35–44]. Recapture takes place only for low photoelectron energy.

In earlier studies, various two-body models, which include a classical model [8], a 'shake-down' model [9, 10], a semiclassical model [11, 12], a quasimolecular adiabatic model [13] and a quantum mechanical model [14–16], have

been used to describe the interaction of the photoelectron with the ion field. Later, other models were used to approximately include the presence of a third particle—an Auger electron. Ogurtsov proposed a new version of a classical model for dealing with cases where the energies of all the electrons are comparable [17]. Junya Mizuno and co-workers studied this problem by solving the classical Coulomb three-body problem [18]. The Niehaus semiclassical model was reformulated in [19], to take into account the time that it takes for the fast Auger electron to overtake the slow electron. The same effect was considered quantum mechanically in papers [45, 46].

Another group of quantum mechanical approaches [3, 4, 6] consider the problem as a three-body problem and take into account the Coulomb interactions between three charged particles: two emitted electrons and a receding ion. These models are applied widely to study PCI effects. Following convention, we refer to them as the SSE (stationary Schrödinger equation) approach models because they are based on the solution of the SSE. The SSE approach allows one to obtain the PCI distorted angle-dependent cross sections. In this paper we select the three most common models within the SSE approach, to investigate: the eikonal approximation [3]; the eikonal approximation with an exact account taken of the electron–electron interaction [4]; and the semiclassical approximation [6]. The three models have been demonstrated to work well in calculating the energy distribution over a wide energy region, and one of the three—the eikonal approximation with an exact account taken of the electron–electron interaction—has been found to yield proper calculations of the angular distribution, except for cases with low photoelectron energy.

As with any quantum mechanical three-body problem, the SSE approach has a limitation arising from the approximate consideration for some of the interactions between each pair of the particles. This approximation is more accurate when the photoelectron is energetic, but has larger uncertainties in systems with low photoelectron energy, and it is poorer if the Auger electron energy is also low. So an approach that can take account of all of the interactions more precisely is needed for this energy region. The approach developed in [1, 2, 47] meets this requirement. It is based on the numerical solution of the time-dependent Schrödinger equation (this is the TDSE approach), free from any physical simplification in interactions between the emitted particles and restricted mainly by the implementation of numerical methods. The aim of this paper is to check the applicability of this recently developed approach [1, 2, 47] (particularly to show its use in the low photoelectron energy region) and test its consistency with the SSE approach. To achieve this aim, we compare the two most important physical quantities in studying the PCI effects: the photoelectron energy and angular distributions, calculated by the TDSE and SSE approaches. Our comparisons are for both low and higher photoelectron energies and we also compare some of our calculations in the low photoelectron energy region with experimental data. Note that carrying out the calculations within the TDSE method and using the numerical implementation of the method discussed, we have restricted ourselves to some approximations which simplify the calculation dramatically and will be discussed in sections 2 and 4. Thus, by combining the TDSE and SSE approaches, the PCI effects can be accurately calculated over an extended range, including the near threshold photoelectron energies.

The energy and angular distributions are mainly determined by three parameters; these are the excess energy of the incident photon above the threshold which is the photoelectron energy, E_1, the Auger electron energy, E_2, and the energy width of the inner vacancy, Γ. E_1 can be adjusted by changing the photon energy, the energy released by the electron which fills the vacancy determines E_2, and Γ is proportional to the inverse of the inner vacancy lifetime. So experimentally, we can choose different values for E_1 while E_2 and Γ are determined by the atomic species. We perform calculations for nine cases in our paper: six of them are real cases for the system of Ne 1 s photoionization followed by KLL Auger decay (where $\Gamma = 0.01$ and $E_2 = 29.4$) and the other three are fictitious cases which have no direct experimental significance but will be very helpful in testing the accuracy of the TDSE approach and highlighting its advantage at low photoelectron energy.

The paper is organized as follows: in section 2 we introduce the TDSE approach briefly; the SSE approach models are discussed in section 3; in section 4 we compare the results calculated by using the TDSE and SSE approaches, and we also compare some of these theoretical results with experimental data; the last section contains our conclusion.

Atomic units are used throughout unless stated otherwise.

2. A brief introduction to the TDSE approach

The TDSE approach is based on the time-dependent close coupling (TDCC) method [47–49]. Modifications to this TDCC method that account for an Auger decay of the inner vacancy were introduced in detail in [1, 2]. This approach allows us to obtain the two-electron wavefunction in real time and we can extract different physical properties from it. This section gives a brief review of this approach.

This TDSE approach is based on the solution of two equations. Equation (1) describes the propagation of the photoelectron before the Auger decay. The photoelectron's wavefunction before the Auger decay will be used as part of the source term of the total wavefunction. This function can be obtained from a time-independent inhomogeneous equation:

$$\left(E_1 + \mathrm{i}\frac{\Gamma}{2} - H_\alpha\right)F_1 = \mathrm{D}\phi_g, \tag{1}$$

where E_1 is the photoelectron energy, $\mathrm{D}\phi_g$ describes the photon absorption of the electron, F_1 is the photoelectron wavefunction, H_α is the Hamiltonian of the photoelectron before the Auger decay and Γ is the width of the inner vacancy. The potential in H_α is taken as $-1/r$ and $\mathrm{D}\phi_g$ is taken

to be a simple short-range function in the calculation; these two approximations are justified for the case studied here because the important interactions take place far outside the core region. Γ is proportional to the inverse of the inner vacancy's lifetime. The wavefunction of the photoelectron, F_1, has the form of a damped continuum wave at energy E_1; the spatial extent of F_1 increases when E_1 increases or Γ decreases.

Equation (2) is the time-dependent Schrödinger equation with a source term for the two ionized electrons after the Auger decay. The two-electron wavefunction $\Lambda(\mathbf{r}_1, \mathbf{r}_2, t)$ is the solution of

$$\mathrm{i}\frac{\partial \Lambda}{\partial t} - H\Lambda = S(t)F_1(r_1)F_2(r_2), \tag{2}$$

where $S(t)$ is the strength of the source, $F_2(r_2)$ is the source term for the Auger electron, and H is the total Hamiltonian. We use $S(t) = 1/\{1 + \exp[10(1 - 5t/t_f)]\}$, where t_f is the final time of the calculation [2]; this form is chosen to make $S(t)$ start at ~0 at $t = 0$ and smoothly transit to 1 well before t_f.

There are three parts in H

$$H = H_1 + H_2 + H_3, \tag{3}$$

where H_1 and H_2 are the Hamiltonian for the photoelectron and the Auger electron respectively, and $H_3 = 1/r_{12}$ is the interaction between the two ionized electrons. The potential in H_1 and H_2 is taken to be $-2/r$, because the ion is doubly charged after the Auger decay; this simple form for the potential works well because the important interactions take place well outside the core.

The two-electron wavefunction Λ can be expressed as

$$\Lambda = \sum_{\ell_1,\ell_2} R^{LS}_{\ell_1\ell_2}(r_1, r_2, t) \sum_{m_1,m_2} C^{\ell_1\ell_2 L}_{m_1 m_2 0} Y_{\ell_1 m_1}(\Omega_1) Y_{\ell_2 m_2}(\Omega_2) \tag{4}$$

where $C^{\ell_1\ell_2\ell_3}_{m_1m_2m_3}$ is a Clebsch–Gordan coefficient, Ω is the solid angle and $Y_{\ell m}(\Omega)$ is a spherical harmonic. In this paper we will consider the case where the two electrons have the same angular momentum: $\ell_1 = \ell_2 = \ell$. (The reason will be given in section 4 when we discuss the limitations and approximations of the TDSE approach.) Then equation (4) is simplified as

$$\Lambda = \sum_{\ell} \frac{(-1)^{\ell}}{\sqrt{4\pi}} R_{\ell}(r_1, r_2, t) Y_{\ell 0}(\cos\theta_{12}) \tag{5}$$

where θ_{12} is the relative angle between the two ionized electrons [1]. Gives the details for how to numerically solve equation (2) and obtain the total wavefunction Λ.

We can extract different physical properties from the two-electron wavefunction Λ. Obviously, the time-dependent position of each electron can be obtained from Λ. At early time, the Auger electron travels behind the photoelectron. After a certain time, the Auger electron will pass the photoelectron and continue ahead of it, perhaps changing the direction of the photoelectron.

With the total wave-function Λ, the energy distribution P_{ϵ_i} can be calculated:

$$A_{\ell}(\epsilon_1, \epsilon_2) = \int\int \mathrm{d}r_1\, \mathrm{d}r_2\, \phi^*_{\epsilon_1\ell}(r_1)\phi^*_{\epsilon_2\ell}(r_2) R_{\ell}(r_1, r_2, t) \tag{6}$$

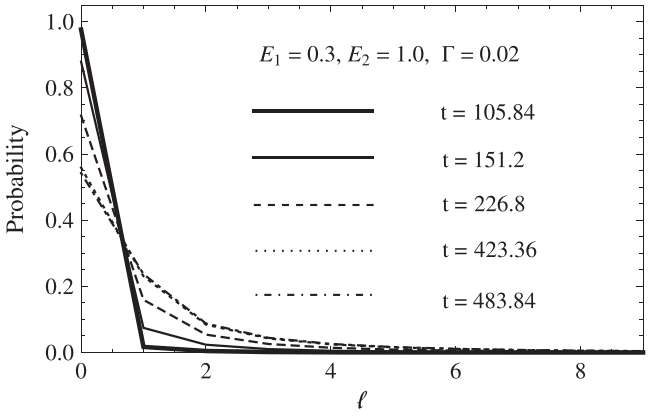

Figure 1. The angular momentum distribution at different times. The wavefunction is mostly at $\ell = 0$ at early time because the two ionized electrons start with zero angular momentum. At later times, the angular momentum of each electron can increase due to the electron–electron interaction. After $t = 423.36$, the Auger electron passes the photoelectron and thus the angular momentum distribution stays the same.

$$P_{\epsilon_i} = \int \mathrm{d}\epsilon_j \sum_{\ell=0}^{\ell_{\max}} \left|A_{\ell}(\epsilon_1, \epsilon_2)\right|^2, \tag{7}$$

where i,j =1,2 and $i \neq j$ (1 and 2 correspond to the photoelectron and Auger electron, respectively), ϵ_i is the always positive energy, P_{ϵ_i} is the energy distribution, and $\phi_{\epsilon_i\ell}(r_i)$ is the electron continuum eigenwavefunction; for the photoelectron, the continuum wave is evaluated in a potential of $-2/r$ while for the Auger electron the potential is $-1/r$.

We can also calculate the angular distribution of the electrons with positive energy. The angle of interest is the relative angle between the two electrons. The angular distribution, $D_k(\cos\theta_{12})$, can be calculated

$$D_k = \int\int \mathrm{d}\epsilon_1\, \mathrm{d}\epsilon_2 \left| \sum_{\ell=0}^{\ell_{\max}} (-1)^{\ell} Y^*_{\ell 0}(\cos\theta_{12}) A_{\ell}(\epsilon_1, \epsilon_2) \right|^2. \tag{8}$$

The angular momentum distribution can be calculated as well

$$P_{\ell} = \int\int \mathrm{d}r_1\, \mathrm{d}r_2 \left|R_{\ell}(r_1, r_2, t)\right|^2. \tag{9}$$

Figure 1 displays the angular momentum distribution at different times. The distribution is concentrated at $\ell = 0$ at early times. With the increase of time, the probability for larger angular momentum increases because the interaction between the two electrons becomes stronger. P_{ℓ} needs to become small for several ℓ values before $\ell_{\max}$.

We use all of the physical quantities to check the convergence of the calculation. For example we can check whether the calculation converges with respect to the time step, the spatial grid width, the energy grid width and the number of angular momenta. Usually larger energy requires a smaller spatial step to achieve convergence because the spatial grid has to be much less than the wavelength of the Auger electron. We also find that cases with a stronger interaction require more angular momenta. The number of angular

momenta is 70 for the case ($E_1 = 0.3$, $E_2 = 1.0$, $\Gamma = 0.02$), to get converged results, and for other cases such as ($E_1 = 0.3$, $E_2 = 29.4$, $\Gamma = 0.01$), 15 are sufficient for the convergence. The interaction between the two electrons is stronger when they have comparable velocities. Also, we can check whether these quantities are converged with respect to time. We extend the calculation time t_f until the physical quantities are no longer changing. Usually, we can obtain converged photoelectron energy and angular momentum distributions at early times in the simulation. It requires more time for the angular and Auger electron energy distributions to converge.

The advantage of the TDSE approach lies in its accuracy in calculating different physical quantities. This is a fully quantum mechanical method, and all of the interactions between each pair of charged particles are considered without any simplification, which is very important when the two emitted electrons propagate with low energies [2]. Displays the angular distribution comparison between the calculation and experimental data for the system of neon 1 s photoionization followed by Auger decay with low photoelectron energy but high Auger electron energy. The good agreement in the comparison demonstrates the validity of this theoretical method in the low photoelectron energy region. Experimental data for cases with both the photoelectron and Auger electron in the low energy region are needed to demonstrate the importance of considering all the interactions precisely.

3. Models for the SSE approach

We will compare results of calculations of the angular and the energy distributions within the TDSE approach with the ones in the framework of the SSE approach. The models that have taken into account the interaction between the receding ion, the photoelectron and the Auger electron and were evaluated within the SSE approach are the eikonal approximation (EIA) [3], the eikonal approach with account taken of the exact interaction between the emitting electrons (EIAEIE) [3, 5], and the semiclassical approximation (SCA) [6]. All of these models present the amplitude of the process as proportional to the integral of overlap between the photoelectron wavefunctions calculated before and after the Auger decay:

$$A \sim \left\langle \psi_k \middle| \psi'_\varepsilon \right\rangle \tag{10}$$

where $\psi_k(\vec{r})$ is the wavefunction of the photoelectron with momentum $\vec{k}$ moving in the field of the doubly charged ion and the Auger electron, and $\psi'_\varepsilon(\vec{r})$ (the F_1 in the TDSE approach) is the photoelectron wavefunction moving in the field of the singly charged ion with the complex energy $\varepsilon - i\Gamma/2$. These functions are calculated via the solution of the stationary Schrödinger equations.

Evaluating an amplitude within the EIA, it is assumed that the interaction of each pair of charged particles (the photoelectron with the ion and the photoelectron with the Auger electron) occurs mainly at large distances where the kinetic energy is much greater than the potential energy of the interacting particles, $W_{kin} \gg W_{pot}$. This condition leads to the limitation of the energies of the slow photoelectron, E_1:

$$E_1 \gg \Gamma^{2/3} \left(E_0/2\right)^{1/3} \tag{11}$$

where E_0 is the atomic unit of energy. On the other hand, the case of similar energies for the photoelectron and Auger electron when they are emitted at small relative angles violates the condition of the applicability of the EIA. Note that the inaccurate account of the interaction of the electrons leads to impossibility of the calculation of the total PCI distortion factor for the angular distribution of the emitted electrons (when it is integrated over all the energies of the emitted electrons) [5].

The EIA was extended to the case where the emitted electrons have comparable velocities and are ejected at small relative angles. In this case, the interaction between the photoelectron and Auger electron has to be taken into account more precisely. This has been done within the EIAEIE [4], where the movement of the photoelectron is considered in the EIA, but the Coulomb interaction between the emitted electrons is taken into account exactly within the quantum mechanical approach. The EIAEIE allows one to calculate the energy and angular distributions of the emitted electrons for a wide range of energies and angles for the ejection of the photoelectron and Auger electron, except for the cases where the condition in equation (11) breaks down.

The semiclassical approximation, SCA, uses the WKB (Wentzel–Kramers–Brillouin) wavefunctions for calculating the overlap integral and leads also to the angle-dependent PCI distortion cross section [6]. It can be applied to the case of low energy photoelectron ejection which lies beyond the condition in equation (11). However, the energy distribution calculation within the SCA method is faced with another restriction, which is

$$0 < v_1/|\mathbf{v}_2 - \mathbf{v}_1| < 1, \tag{12}$$

where $\mathbf{v}_1$, $\mathbf{v}_2$ are the velocities of the photoelectron and Auger electron, respectively. If the relative velocity of the emitted electrons is small and they lie in the region where $v_1/|\mathbf{v}_2 - \mathbf{v}_1| > 1$, the SCA approach cannot be used. This restriction is connected to the fact that the point of the stationary phase (this method is used for evaluation of the overlap integral) in the region considered is going to infinity and the stationary phase method breaks down.

An advantage of the SSE approach is the fact that all three models considered here give analytical expressions for the amplitudes and cross sections that can be used for analysis and calculation of the energy and angular distributions over a wide region of energies and angles of electron emission. A numerical implementation of these formulas is straightforward and reduces to the calculation of some special functions in the complex plane. Note that calculations within the models considered for the SSE approach carried out in the region of their applicability give results that agree quite well with measurements both of energy distributions (see e.g. [20]) and of angular distributions [25, 26, 30]. So the line shapes of the 2.7 eV 4d photoelectrons in Xe ($\Gamma = 110$ meV) calculated

within the EIA approach agree very well with the measured energy distributions in papers [20] and [50]. Also the energy distributions of the 2p photoelectrons in Ar ($\Gamma = 118$ meV) calculated by using the EIA model agree well with the measured ones for the excess photon energies 3 eV, 9 eV and 12 eV but disagree for the excess energy 0.85 eV [33]. However, the calculation within the SCA approach [21] shows good agreement with experimental data in this case. The angle-dependent energy distributions of the 30.5 eV electrons in the Xe 4d ionization followed by the $N_5O_{23}O_{23}$ Auger decay were measured in coincidence with the Auger electrons [25, 26] and show good agreement with the calculation within the EIA approach. The angular distribution of the 17 eV 4d photoelectrons in Xe was measured in coincidence with the 30 eV $N_5O_{23}O_{23}$ Auger electrons [30] and shows good agreement with the calculations within the EIAEIE. The angular distribution of the 13.5 eV 2 s photoelectrons emitted due to the resonance photoionization in neon and followed by Auger decay ($Ne^{+*}(2s2p^5(^3P)3p(^2S)) \rightarrow Ne^{2+}(2\,s^2 2p^4(^1D)) + e_A$, where the Auger electron has similar energy to the photoelectron) was calculated by using the EIAEIE in [28], and the agreement between the calculations and measurements is quite reasonable.

4. Comparison between the results from the TDSE and SSE approaches

In this section, we compare the photoelectron energies and angular distributions for several cases calculated by using the two different quantum mechanical approaches: TDSE and SSE. This comparison will highlight the agreement and disagreement of results obtained by various methods. Note that some approximations are made in the TDSE approaches. For example, we use $-Z/r$ as the potential in the Hamiltonian. This approximation is accurate when the photoelectron travels far from the nucleus before it interacts with the Auger electron. For very low photoelectron energy ($E_1 \approx 0$), the approximation will not be as accurate. We use a different potential, $-(Z + (10 - Z)\exp(-r/r_a))/r$ (r_a is atomic radius, and it is 0.71 for neon) in the calculation and find that the results with this potential are the same as those with the potential $-Z/r$ except for the situation when the initial photoelectron energy is very close to 0. Another approximation is that in which the expressions for $D\phi_g$ in equation (1) and $F_2(r_2)$ in equation (2) are replaced by two simple short-range functions. As with the simple approximation to the Hamiltonian, this approximation breaks down for 0 initial photoelectron energy or large Γ. We also assume that both ionized electrons start with 0 angular momentum. This approximation is not necessary, but it simplifies the calculation dramatically and allows us to use the available computer capacities and to carry out the calculation in reasonable time. This restriction means that cases with nonzero total angular momentum L are not treated in the current TDSE calculations. However, we expect the general trends for other total angular momenta to be similar to those in this paper because the electrons are at large distance when the interaction occurs. We plan to perform calculations with different total angular momentum in future work by using more refined numerical methods. The main limitation of the TDSE approach is the computer capacity. If an electron's energy is larger, a greater number of points for the radial grid is needed to get a converged result; if two electrons have comparable velocities, more angular momenta are required in the calculation. So the TDSE approach breaks down when both of the ionized electrons have very large velocities or have large and comparable velocities.

The SSE approach contains three different approximations for calculating the energy distribution. The first is the EIA which works for cases where the two ionized electrons have large and different velocities and the relative angle between them is not too small. When the two ionized electrons have large and comparable velocities or the Auger electron is launched near the direction of the photoelectron, the second approximation, the EIAEIE, should be applied. The condition in equation (11) can be used to test whether the EIA or the EIAEIE approximation is accurate. The third approximation is the SCA, which is accurate for low excess photoelectron energy. The condition in equation (12) has to be satisfied for this semiclassical approximation. In this paper, only the EIAEIE approximation is applied to calculate the angular distribution. The EIA fails in the calculation of the angular distribution because the interaction between the two ionized electrons is the main reason for the distortion in the angular distribution [5]; the EIA is used when three particles are far apart and their trajectories are a straight line, so the angular distribution calculated by using the EIA has little PCI distortion. The reason for not calculating the angular distribution using the SCA is similar, because the interaction between the two ionized electrons is not fully considered in this approximation either. The PCI distortion factor for the angular distribution given by the EIA approach was shown to be strongly equal to 1 (see [5]), and we have a similar conclusion for the SCA, which has been checked by direct numerical calculation.

For the system studied here, a close comparison between theoretical methods, and with experiment, is critical for developing a full picture of the dynamics. In the following subsections we compare a range of theoretical calculations. At the end of each section we also compare with available experimental data.

4.1. Comparison of the photo-electron energy distributions

First we examine the photoelectron energy distributions. Four typical cases are selected for discussing the similarity and distinction of results obtained by various approaches. We will also investigate the differences between the results, relating them to the restrictions of these approaches.

The first two cases are Case 1A ($E_1 = 0.0735$, $E_2 = 2.0$, $\Gamma = 0.01$) and Case 2A ($E_1 = 0.1$, $E_2 = 29.4$, $\Gamma = 0.01$). For Cases 1A and 2A, the right-hand side of the condition in equation (11) is

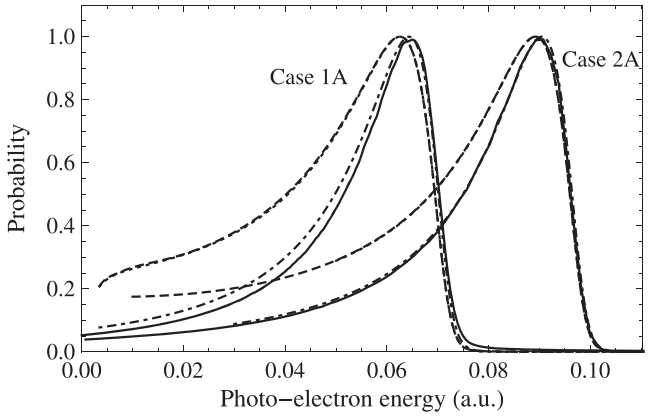

Figure 2. The photoelectron energy distribution comparison for different approaches for two cases. The left curves are for Case 1A ($E_1 = 0.0735$, $E_2 = 2.0$, $\Gamma = 0.01$), and the right curves are for Case 2A ($E_1 = 0.1$, $E_2 = 29.4$, $\Gamma = 0.01$). For both cases the dotted line is for the calculation obtained using the EIA of the SSE approach, the dashed line is for the EIAEIE approximation, the dot–dashed line is for the SCA and the solid line is the result obtained using the TDSE approach.

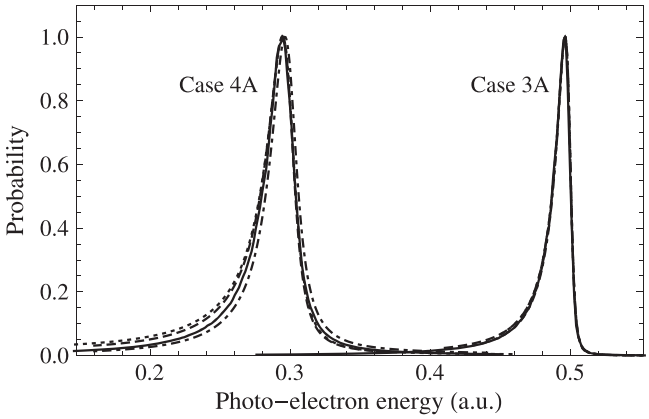

Figure 3. The photoelectron energy distribution comparison for different approaches for two cases. The left curves are for Case 4A ($E_1 = 0.3$, $E_2 = 1.0$, $\Gamma = 0.02$), and the right curves are for Case 3A ($E_1 = 0.5$, $E_2 = 29.4$, $\Gamma = 0.01$). For both cases the dotted line is for the calculation obtained using the EIA of the SSE approach, the dashed line is for the EIAEIE approximation, the dot–dashed line is for the SCA and the solid line is the result obtained using the TDSE approach.

$0.01^{2/3}(1/2)^{1/3} \approx 0.0368$. E_1=0.0735 in Case 1A and 0.1 in Case 2A. Neither of the two values is much larger than 0.0368. So the EIA and the EIAEIE approximation should not work well. However, the value of $v_1/|\mathbf{v}_2 - \mathbf{v}_1|$ in the condition in equation (12) is approximately 0.161–0.237 for Case 1A and 0.055–0.062 for Case 2A. The two ranges are both between 0 and 1, and the SCA should give accurate results. As shown in figure 2, the PCI distortions in the EIA and in the EIAEIE approximation are much larger than those in the TDSE approach and the SCA: the shift of the distribution maximum is larger and the left wing of the distribution broadens strongly. This is connected with the violation of the condition in equation (11) in the near threshold region and with underestimation of the potential energy. It leads to a stronger influence of the ionic field variation on the photoelectron propagation, and consequently on the PCI distortion. As the photoelectron energy decreases, the discrepancy between the calculations increases. The disagreement between the results within the EIA and within the SCA was first noted in [6]. For both cases, the results obtained with the SCA agree much better with those from the TDSE approach. The agreement in Case 2A is better than that in Case 1A, and the discrepancy lies in the left wing of the distribution in both cases. These small disagreements can be connected with the approximations which were used in the evaluation of the SCA [6]. The results obtained using the EIA and using the EIAEIE approximation almost coincide in these two cases. Because the velocities of the two electrons are not very close to each other, whether one considers the interaction between the two emitted electrons exactly or not makes little difference to the results.

The other two cases selected for discussing the photoelectron energy are Case 3A ($E_1 = 0.5$, $E_2 = 29.4$, $\Gamma = 0.01$) and Case 4A ($E_1 = 0.3$, $E_2 = 1.0$, $\Gamma = 0.02$). The condition in equation (11) is satisfied for both cases: $0.5 \gg 0.0368$ for Case 3A and $0.3 \gg 0.0585$ for Case 4A. The value of $v_1/|\mathbf{v}_2 - \mathbf{v}_1|$ is approximately 0.115–0.150 for Case 3A and 0.354–1.211 for Case 4A. Case 3A fully satisfies the condition in equation (12) but Case 4A fails for some angles ($0.913 < \cos\theta_{12} < 1$). In Case 3A (the right part of figure 3), the three different SSE approximations give the same photoelectron energy distribution because both the conditions in equation (11) and those in equation (12) are satisfied, and they agree quite well with those from the TDSE approach. In Case 4A (the left part of figure 3), the four results are also close although none of the SSE approximations agree perfectly with the TDSE result. The result from the TDSE approach agrees best with that obtained using the EIAEIE approximation because the condition in equation (12) is not satisfied for some angles and the two electrons have comparable large velocities. The small difference between the TDSE approach and the EIAEIE approximation results is also found in the left wing because the condition in equation (11) is not satisfied in the low energy range.

Our theoretical findings can be verified by the available measurements [32]. Figure 4 presents the theoretical and experimental energy distribution comparison for the case ($E_1 = 0.05$, $E_2 = 29.4$, $\Gamma = 0.01$). The results calculated within the EIA (the thin solid line) and within the EIAEIE approximation (the dashed line) coincide with each other, but significantly deviate from the experimental data [32] (symbolized by dots in figure 4). This is what we expected, because this case violates the condition in equation (11) (E_1 is comparable with the value $0.01^{2/3}(1/2)^{1/3} \approx 0.0368$). However, the condition of equation (12) is satisfied (the value of $v_1/|\mathbf{v}_2 - \mathbf{v}_1|$ is 0.0396–0.043), and the result calculated using the SCA should be more accurate. The results from the TDSE method (the thick solid line) and obtained using the SCA (the dot–dashed line) agree with each other. They also fit well with the experimental data, and the agreement in the low energy region is better than that in the higher energy region. The

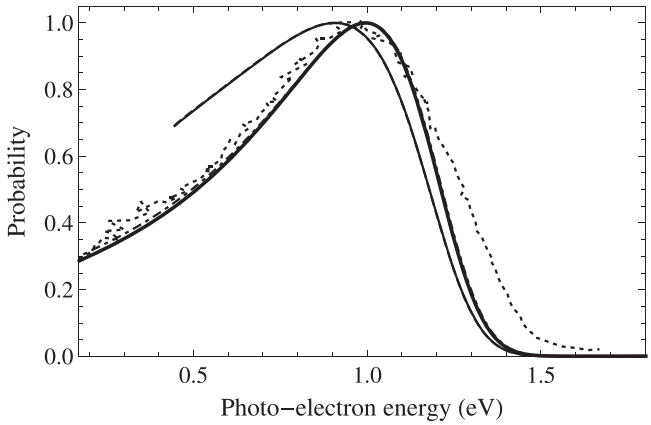

Figure 4. The photoelectron energy distribution comparison for theoretical calculations and experimental data for the case of 1 s photoionization of Ne ($E_1 = 0.05$, $E_2 = 29.4$, $\Gamma = 0.01$). The dotted line is for the experimental measurement extracted from [32], the thin solid line is for the calculation obtained using the EIA of the SSE approach, the dashed line is for the EIAEIE approximation, the dot–dashed line is for the SCA and the thick solid line is the result from the TDSE approach.

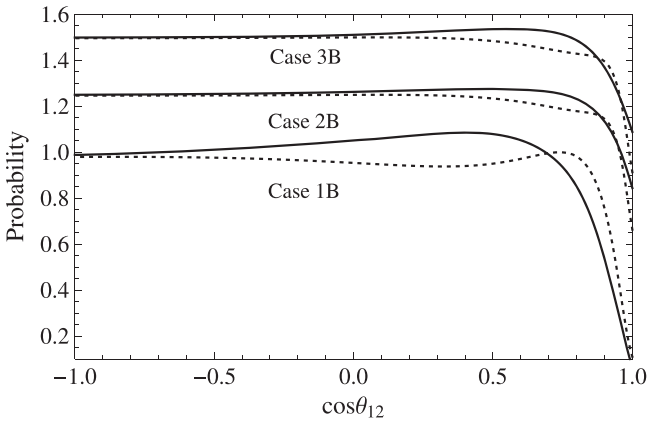

Figure 5. The angular distribution comparison for the two approaches for three cases. The solid lines for the three cases show the calculations obtained using the TDSE approach, and the dotted lines are for the SSE approach. Case 1B is ($E_1 = 0.0735$, $E_2 = 2.0$, $\Gamma = 0.01$), Case 2B (shifted up by 0.25) is ($E_1 = 0.0735$, $E_2 = 29.4$, $\Gamma = 0.01$) and Case 3B (shifted up by 0.5) is ($E_1 = 0.05$, $E_2 = 29.4$, $\Gamma = 0.01$).

difference between the experimental data and the SCA or the TDSE curve may be caused by a yield of occasional electrons (via the capture and re-emission of slow photoelectrons) which are recorded experimentally but not included in the calculations here. Another possible reason for this small disagreement may be associated with the photon energy resolution which is also not included in the calculation. For the resolution of the electron spectrometer, we simulate this function by the Gaussian with permanent FWHM = 170 meV [32] for all energies of the calculation range. However, the real experimental function may differ from the function that we used and have a more complicated form. That is also a possible reason for the disagreement.

4.2. Comparison of the angular distributions

To investigate the angular distribution, we selected cases designed for comparing the TDSE approach and the EIAEIE approximation. Any difference between the two approaches should be related to the photoelectron energy E_1 and the Auger width Γ because of the condition in equation (11). However, we found that the TDSE approach and the EIAEIE gave closer results for larger Auger electron energy, which suggests an approximation beyond that captured by the condition in equation (11).

Cases with low excess photoelectron energy cannot satisfy the condition in equation (11), so the angular distribution calculated by the EIAEIE and by the TDSE approach should be expected to have a notable difference. With the increase of the photoelectron energy, the agreement between the two approaches becomes better. For cases with low photoelectron energy, if the Auger electron energy is also small, the agreement between the two methods is poorer, as compared to cases with larger Auger electron energy. Figure 5 shows the comparison of the angular distribution for the three cases. The solid lines are the results from the TDSE approach and the dotted lines are the results from the SSE approach. Case 2B ($E_1 = 0.0735$, $E_2 = 29.4$, $\Gamma = 0.01$) has the same Γ and E_2 as Case 3B ($E_1 = 0.05$, $E_2 = 29.4$, $\Gamma = 0.01$), but a different E_1. For these two cases, the test for the condition in equation (11) is $0.0735 \gg 0.0368$ for Case 2B and $0.05 \gg 0.0368$ for Case 3B. Neither of these satisfies the condition, and as a result the SSE approach does not agree very well with the TDSE approach. Case 2B has the same Γ and E_1 as Case 1B ($E_1 = 0.0735$, $E_2 = 2$, $\Gamma = 0.01$), but a quite different E_2. The condition in equation (11) fails in both cases. However, the error in Case 1B is much larger than that in Case 2B because the Auger energy is much smaller.

One reason for this phenomenon may be that the distortion in the angular distribution is mainly caused by the electron–electron interaction which has been considered exactly in the EIAEIE approximation. The interaction between the ion and photoelectron or Auger electron also plays some role in the angular distribution. When the Auger electron has very high energy, the eikonal approximation for the ion–Auger electron interaction used in the EIAEIE approximation is valid, and causes little error. This is the other possible reason for this phenomenon. Thus, we can conclude that, unlike for the energy distribution case, the angular distribution calculated by using the EIAEIE approximation can be more accurate or close to the TDSE result in a case with low photoelectron energy (i.e. where the condition in equation (11) is not satisfied) but very high Auger electron energy.

For cases with high photoelectron energy, the agreement between the TDSE approach and the SSE approach is better. This is what we expect, because the condition in equation (11) is satisfied here, and the EIAEIE approximation works well. We divide this energy region into two scenarios. When the two electrons have quite different energies, the disagreement between the two methods lies in the small angle region, which can be shortened if we increase the photoelectron energy.

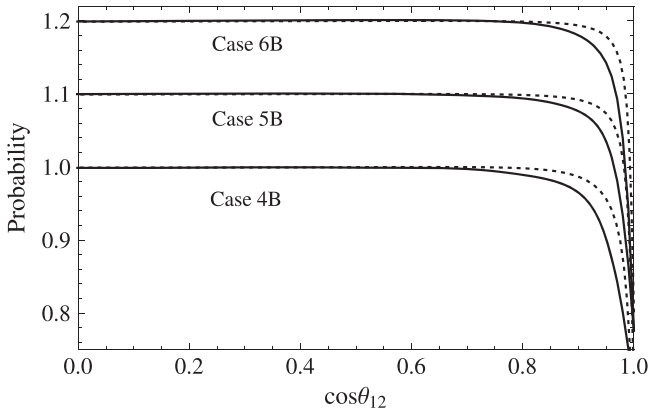

Figure 6. The angular distribution comparison for the two approaches for another three cases. The solid lines for the three cases show the calculations obtained using the TDSE approach, and the dotted lines are for the SSE approach. The two approaches agree well. Case 4B is ($E_1 = 0.3$, $E_2 = 29.4$, $\Gamma = 0.01$), Case 5B (shifted up by 0.1) is ($E_1 = 0.4$, $E_2 = 29.4$, $\Gamma = 0.01$) and Case 6B (shifted up by 0.2) is ($E_1 = 0.5$, $E_2 = 29.4$, $\Gamma = 0.01$).

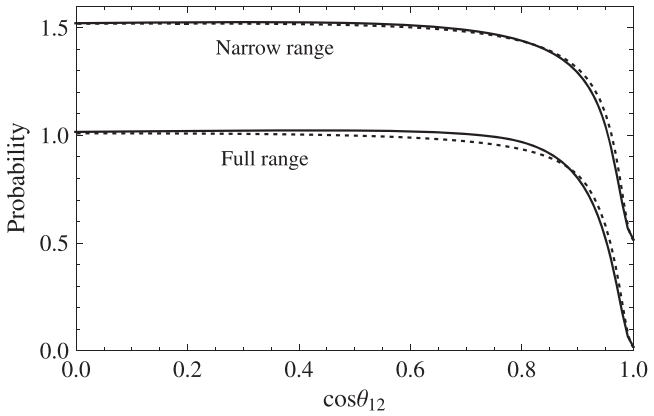

Figure 7. The angular distribution comparison for the two approaches for the case ($E_1 = 0.5$, $E_2 = 2.0$, $\Gamma = 0.02$) with different photoelectron energy integration ranges. The solid lines of the ranges are for the calculation obtained using the TDSE approach, and the dotted lines are for the SSE approach. The curves marked 'Narrow range' and 'Full range' correspond to the photoelectron energy integration ranges 10–15 eV and 6.2–18 eV, respectively.

figure 6 shows the angular distribution comparison for three cases. They are Case 4B ($E_1 = 0.3$, $E_2 = 29.4$, $\Gamma = 0.01$), Case 5B ($E_1 = 0.4$, $E_2 = 29.4$, $\Gamma = 0.01$) and Case 6B ($E_1 = 0.5$, $E_2 = 29.4$, $\Gamma = 0.01$). These three cases have the same E_2 and Γ but different E_1. The E_2 in all three cases is much larger than E_1. The right-hand side of the condition in equation (11) is approximately 0.0368 for all three cases, which means that the condition in equation (11) is fully satisfied. So the two approaches agree better in the three cases. The difference between the two approaches starts from $\cos\theta_{12} = 0.74$ in Case 4B, 0.80 in Case 5B and 0.85 in Case 6B. Case 6B has the smallest discrepancy angle range due to its highest E_1. It is unclear where the difference comes from and which method works better for this situation; it may be connected either with the limitation of adopting $L = 0$ in our version of the TDSE approach or with inaccuracies of the EIAEIE method in this region.

As for the second situation, when the two electrons have comparable energies, the difference between the two approaches lies in the position where the angular distribution starts to decrease. The difference for this situation is mainly caused by the inaccuracy of the EIAEIE approximation for small photoelectron energy and by the range of the photoelectron energies included in the consideration. We get such a conclusion because the difference is smaller when we recalculate the angular distribution with narrower photoelectron energy integration range (smaller photoelectron energy is excluded in this range). Figure 7 shows the angular distribution comparison for the case ($E_1 = 0.5$, $E_2 = 2.0$, $\Gamma = 0.02$) with two different photoelectron energy integration ranges. Substituting values into the condition in equation (11) gives $0.5 \gg 0.0585$, which indicates that the EIAEIE approximation should work well. Agreement between the two methods is better when the photoelectron energy integration range is narrow, 10–15 eV, and the difference becomes larger when we integrate the

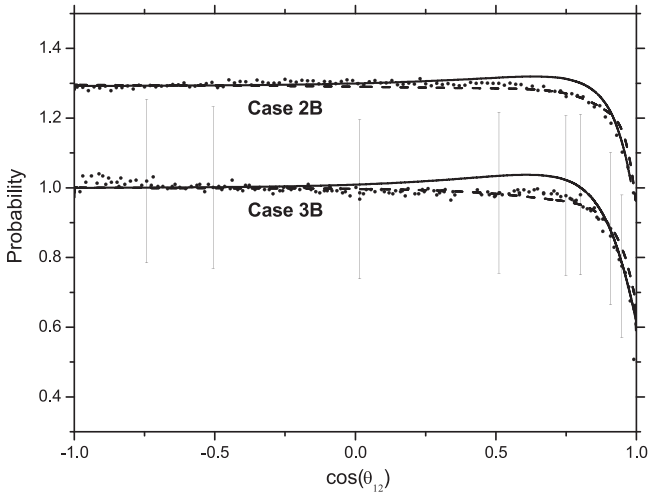

Figure 8. The angular distribution comparison for the theoretical calculations and experimental data for 1 s photoionization of Ne. The dotted lines show the experimental measurements from [2] (Case 2B) and [32] (Case 3B), the solid line is for the calculation obtained using the TDSE approach, and the dashed line is for the SSE approach. The error bars for the statistical inaccuracy are shown for a few points for case 3B. Case 3B is ($E_1 = 0.05$, $E_2 = 29.4$, $\Gamma = 0.01$); Case 2B (shifted up by 0.3) is ($E_1 = 0.0735$, $E_2 = 29.4$, $\Gamma = 0.01$).

photoelectron energy from 6.2 to 18 eV because some low photoelectron energies (after the Auger decay) do not satisfy the condition in equation (11).

In the final part of the angular distribution investigation, we select two cases (2B ($E_1 = 0.0735$, $E_2 = 29.4$, $\Gamma = 0.01$) and 3B ($E_1 = 0.05$, $E_2 = 29.4$, $\Gamma = 0.01$)) in order to compare the angular distributions calculated from theories and that measured experimentally. The comparison for Case 2B shown in figure 8 meets our expectation. The TDSE calculation (the solid line) agrees well with the experimental measurement (the dotted line) [2]. Though the condition in equation (11) is not satisfied in this case, the EIAEIE curve (the dashed line) fits the experimental data nicely. One

possible reason is that the inaccuracy of the angular distribution calculated by using the EIAEIE approximation is small if the initial Auger electron energy is very high, which has been discussed above. The other reason may be that the integration range of the photoelectron energy for Case 2B is 0.5–2.5 eV; very low photoelectron energies are not included in calculations, which reduces the error of the EIAEIE approximation.

Generally, the theoretical calculations also agree with the experimental data in the comparison for Case 3B displayed in figure 8. Note that the integration range for the photoelectron energy is 0.1–2.0 eV for the calculated curves, and the theoretical curves were convoluted with a Gaussian with a FWHM of 2.2° [32]. One surprising result is that the deviation of the results obtained by the TDSE method from the experimental data (the dotted line) [32] is larger than that for the EIAEIE calculation, although the TDSE and EIAEIE curves both agree reasonably well with the measured dependence. This unexpected phenomenon can be explained by two features. Firstly, the interaction between the photoelectron and the Auger electron, which is taken into account exactly in EIAEIE calculations, is the main factor in determining the shape of the angular distribution. Our calculation within the EIAEIE neglects the capture of slow photoelectrons, which is important at very low photoelectron energies, and could influence the angular distribution under certain experimental conditions (see, e.g., [40]). However the measurements [32] do not satisfy these conditions and the EIAEIE results agree quite well with the experimental data. Secondly, our calculations in this paper within the TDSE approach take into account only the angular momentum $L = 0$ of the pair of emitted electrons. However for the Ne 1 s case the other momenta $L = 1, 2, 3$ can contribute to the electron's emission and slightly change the angular distribution.

5. Conclusion

In this paper, we performed calculations for different cases within two groups of quantum mechanical approaches. After comparing the calculated and measured photoelectron energy and angular distributions, we made the following generalizations.

For cases with low photoelectron energy, the TDSE approach describes well both the photoelectron energy and the angular distributions. The SCA for the SSE approach gives a similar photoelectron energy distribution to the TDSE approach if the condition for its applicability is satisfied. The other two approximations of the SSE approach, the EIA and the EIAEIE approximation, are not accurate for the energy distribution because the condition for their applicability usually cannot be satisfied in this energy region. The EIAEIE approximation has less inaccuracy in its angular distribution than its energy distribution if the Auger electron has very high energy.

For cases with medium to high photoelectron energy, the EIAEIE approximation of the SSE approach describes well both the photoelectron energy and the angular distributions. All the three models for the SSE approach give similar energy distributions as long as the conditions for their applicability are satisfied. The TDSE approach is suitable for use in calculating both the photoelectron energy and the angular distributions in this energy region. The agreement between the results from the two approaches is excellent for the photoelectron energy distribution. For the angular distributions, there are only small differences between the results from the two methods. The TDSE approach may break down if both electrons have high and comparable energies. In this case larger numbers of angular momenta and radial mesh points are required to get the converged results, requiring very large computational resources.

For cases where both electrons have very high energies, the SSE approach can be applied for both the energy and the angular distributions, and the TDSE approach breaks down because of the requirement for a huge number of points in the calculation.

By considering an energy region where both methods are applicable, it has been shown that, together, the TDSE and SSE approaches cover almost all of the energy range for which people might be interested in studying PCI effects. Our theoretical methods are confirmed by the agreement with measurements of the energy and angular distributions of the 1 s photoelectrons emitted from Ne. More precise agreement of the results from the TDSE approach and measured angular distributions can be reached both by including higher total angular momenta in the calculation and by carrying out measurements with less statistical inaccuracy.

Acknowledgements

This material is based upon work supported by the US Department of Energy Office of Science, Office of Basic Energy Sciences, Chemical Sciences, Geosciences, and Biosciences Division under Award Number DE-SC0012193.

References

[1] Robicheaux F 2012 *J. Phys. B: At. Mol. Opt. Phys.* **45** 135007
[2] Robicheaux F, Jones M P, Schoffler M *et al* 2012 *J. Phys. B: At. Mol. Opt. Phys.* **45** 175001
[3] Kuchiev M Y and Sheinerman S A 1986 *Sov. Phys.-JETP* **63** 1680
[4] Kuchiev M Y and Sheinerman S A 1988 *J. Phys. B: At. Mol. Opt. Phys.* **21** 2027
[5] Kuchiev M Y and Sheinerman S A 1994 *J. Phys. B: At. Mol. Opt. Phys.* **27** 2943
[6] van der Straten P, Morgenstern R and Niehaus A 1988 *Z. Phys.* D **8** 35
[7] Kuchiev M Y and Sheinerman S A 1989 *Sov. Phys. Usp* **32** 569
[8] Barker R B and Berry H W 1966 *Phys. Rev.* **151** 14
[9] Read F H 1975 *Radiat. Res.* **64** 23
[10] King G C, Read F H and Bradford R C 1975 *J. Phys. B: At. Mol. Opt. Phys.* **8** 2210

[11] Niehaus A 1976 *J. Phys. B: At. Mol. Opt. Phys.* **10** 1845
[12] Helenelund K, Hedman S, Asplund L, Gelius U and Siegbahn K 1983 *Phys. Scr.* **27** 245
[13] Ostrovskii V N 1977 *Sov. Phys.-JETP* **45** 1092
[14] Amus'ya M Y, Kuchiev M Y and Sheinerman S A 1979 *Sov. Phys.-JETP* **49** 238
[15] Kuchiev M Y and Sheinerman S A 1985 *J. Phys. B: At. Mol. Opt. Phys.* **18** L551
[16] Tulkki J, Armen G B, Å berg T, Crasemann B and Chen M H 1987 *Z. Physik* D **5** 241
[17] Ogurtsov G N 1983 *J. Phys. B: At. Mol. Opt. Phys.* **16** L745
[18] Mizuno J, Ishihara T and Watanabe T 1985 *J. Phys. B: At. Mol. Opt. Phys.* **18** 1241
[19] Russek A and Mehlhorn W 1986 *J. Phys. B: At. Mol. Opt. Phys.* **19** 911
[20] Sheinerman S A, Lablanquie P, Penent F *et al* 2006 *J. Phys. B: At. Mol. Opt. Phys.* **39** 1017
[21] Gerchikov L and Sheinerman S 2011 *Phys. Rev.* A **84** 022503
[22] Schmidt V, Sandner N, Mehlhorn W, Adam M Y *et al* 1977 *Phys. Rev. Lett.* **38** 63
[23] Bahl M K, Watson R L and Irgollic K J 1979 *Phys. Rev. Lett.* **42** 165
[24] Lohmann B, Meng X K and Keane M 1992 *J. Phys. B: At. Mol. Opt. Phys.* **25** 5223
[25] Kämmerling B, Krässig B and Schmidt V 1993 *J. Phys. B: At. Mol. Opt. Phys.* **26** 261
[26] Avaldi L, Belotti P, Bolognesi P, Camilloni R and Stefani G 1995 *Phys. Rev. Lett.* **75** 1915
[27] Kassühlke B, Romberg R, Averkamp P and Feulner P 1998 *Phys. Rev. Lett.* **81** 2771
[28] Sheinerman S and Schmidt V 1999 *J. Phys. B: At. Mol. Opt. Phys.* **32** 5205
[29] Rioual S *et al* 2001 *Phys. Rev. Lett.* **86** 1470
[30] Scherer N, Lörch H, Kerkau T and Schmidt V 2004 *J. Phys. B: At. Mol. Opt. Phys.* **37** L121
[31] Penent F *et al* 2005 *Phys. Rev. Lett.* **95** 083002
[32] Landers A L *et al* 2009 *Phys. Rev. Lett.* **102** 223001
[33] Sheinerman S *et al* 2010 *J. Phys. B: At. Mol. Opt. Phys.* **43** 115001
[34] Guillemin R, Sheinerman S, Bomme C *et al* 2012 *Phys. Rev. Lett.* **109** 013001
[35] van der Wiel M J, Wight G R and Tol R R 1976 *J. Phys. B: At. Mol. Opt. Phys.* **9** L5
[36] Ya Amusia M, Yu Kuchiev M, Sheinerman S A and Sheftel S I 1977 *J. Phys. B: At. Mol. Opt. Phys.* **10** L535
[37] Eberhardt W, Bernstorff S, Jochims H W, Whitfield S B and Crasemann B 1988 *Phys. Rev.* A **38** 3808
[38] Tulkki J, Åberg T, Whitfield S B and Crasemann B 1990 *Phys. Rev.* A **41** 181
[39] Armen G B and Levin J C 1997 *Phys. Rev.* A **56** 3734
[40] Sheinerman S A 2003 *J. Phys. B: At. Mol. Opt. Phys.* **36** 4435
[41] Fanis A D *et al* 2004 *Phys. Rev.* A **70** 040702
[42] Sheinerman S A 2005 *J. Phys. B: At. Mol. Opt. Phys.* **38** 2279
[43] Fanis A D, Prümper G, Hergenhahn U *et al* 2005 *J. Phys. B: At. Mol. Opt. Phys.* **38** 2229
[44] Hergenhahn U, Fanis A D, Prümper G *et al* 2005 *J. Phys. B: At. Mol. Opt. Phys.* **38** 2843
[45] Koike F 1988 *J. Phys. Soc. Japan* **57** 2705
[46] Armen G B, Tulkki J, Aberg T and Crasemann B 1987 *Phys. Rev.* A **36** 5606
[47] Pindzola M S, Robicheaux F, Loch S D *et al* 2007 *J. Phys. B: At. Mol. Opt. Phys.* **40** R39
[48] Hochstuhl D and Bonitz M 2011 *J. Chem. Phys.* **134** 084106
[49] Hochstuhl D and Bonitz M 2012 *Phys. Rev.* A **86** 053424
[50] Palaudoux J, Lablanquie P, Andric L *et al* 2008 *J. Phys.: Conf. Ser* **141** 012012